International Journal of Heat and Mass Transfer 51 (2008) 5542–5551

Contents lists available at ScienceDirect

International Journal of Heat and Mass Transfer

journal homepage: www.elsevier.com/locate/ijhmt

Effects of gender-related geometrical characteristics of aorta–iliac bifurcation on hemodynamics and macromolecule concentration distribution

Mehrzad Khakpour, Kambiz Vafai *

Mechanical Engineering Department, University of California, Riverside, CA 92521, USA

ARTICLE INFO

Article history:
Received 5 February 2008
Received in revised form 4 April 2008
Available online 6 June 2008

Keywords:
Hemodynamics
Macromolecule transport
Aorta–iliac bifurcation
Gender
Asymmetry

ABSTRACT

Aorta–iliac bifurcation has been anatomically shown to be asymmetric. Also, statistical data reveal differences in the structural features of average male and female aorta–iliac bifurcation. In the present work, numerical simulations of the macromolecule transport at the aorta–iliac bifurcation are performed. The transport phenomena within the lumen and the arterial wall are coupled. The arterial wall is modeled as a four-layer porous wall, representing endothelium, intima, internal elastic lamina (IEL), and media layers. The layers are all treated as macroscopically homogeneous porous media with uniform morphological properties. The Staverman filtration coefficient is incorporated to account for selective permeability of each porous layer to macromolecules. Different geometrical attributes of the aorta–iliac bifurcation are studied, i.e. asymmetry and gender-dependence. Profiles of macromolecule concentration distributions are obtained for different cases. The results are discussed with regard to the shear stress distribution, which is believed to be one of the key factors in atherogenesis. The present study appears to be the first one to discuss the effects of gender and geometrical characteristics (e.g. asymmetry) on the transport phenomena at the aorta–iliac bifurcation.

1. Introduction

Cardiovascular diseases are the leading cause of death in the United States [1]. Most cardiovascular complications are secondary to atherosclerosis. Among the complications of atherosclerosis are heart attacks, strokes, angina, ischemia, thromboembolisms, and aneurysms. Atherosclerosis is a systemic, proliferative and inflammatory disease of the arterial wall and usually occurs in large and medium-sized muscular arteries. It is a progressive disorder that may take decades to develop. It is associated with and is characterized by several pathophysiological phenomena such as endothelial dysfunction, lipid accumulation, vascular inflammation, proliferation of vascular smooth muscle cells, and plaque formation, and it eventually leads to blood supply disruption and other cardiovascular diseases [2]. A complete description of atherogenesis and its step-by-step progression towards atherosclerosis is provided by Glass and Witztum [3].

Medical data shows that the atherosclerosis lesions do not occur at random [4,5]. They usually develop at the sites of branching, bifurcation, bending, and local dilation. As such, the coronary arteries, the major branches of the aortic arch, and the abdominal aorta and its abdominal and major lower extremity branches are particularly susceptible sites [4]. Hemodynamic forces interacting with an active vascular endothelium are believed to be largely responsible for localizing lesions in a nonrandom pattern of distribution [5]. Shear stress and cyclic circumferential strain are the predominant forces that have been characterized. In addition to its influence on endothelial function, hemodynamics may alter the local concentration of LDL within the arterial wall.

To date, modeling the development and progression of atherosclerosis has been quite challenging. However, important factors involved in its initiation and localization may be studied through theoretical and/or computational modeling of the underlying transport phenomenon. At its early stages, atherosclerosis predominantly involves the inner layers (endothelium and intima) of an artery [3]. Aside from the complex pathophysiological interactions between the cellular elements (endothelial cells, smooth muscle cells, platelets, and leucocytes) of the atherosclerotic lesion, the process can be considered as a transport phenomenon [6–8]. Accurate modeling of this phenomenon requires utilization of a comprehensive arterial model, which provides a precise description of the anatomy of arteries. A critical assessment of the arterial transport models along with the governing equations and boundary conditions is provided by Khakpour and Vafai [8].

A great majority of previous studies employed a wall-free arterial transport model [8] and focused on the hemodynamics and rheology of blood flow within the arteries as well as the polarization of LDL concentration at the lumen–endothelium interface. In these studies, the arterial wall itself was not modeled. Instead, a set of boundary conditions (e.g. constant filtration velocity) was utilized to represent the arterial wall. Although useful in providing

* Corresponding author. Tel.: +1 951 827 2135; fax: +1 951 827 2899.
E-mail address: vafai@engr.ucr.edu (K. Vafai).

0017-9310/$ - see front matter © 2008 Elsevier Ltd. All rights reserved.
doi:10.1016/j.ijheatmasstransfer.2008.04.025

Nomenclature

C	macromolecule concentration
c	non-dimensional macromolecule concentration
D	mass diffusion coefficient
d	diameter
K	permeability
k	reaction rate
L	length
$\vec{n}$	unit vector normal to interface
p	pressure
R	radius
Re	Reynolds number=$\frac{u_m d_a}{\upsilon}$
r	radial location
$\vec{t}$	unit vector tangential to interface
u	x component of velocity vector
u_m	mean value of x component of velocity vector
$u_{\max}$	centerline value of x component of velocity vector
$\vec{V}$	velocity vector

Greek symbols

α	bifurcation angle
δ	porosity
μ	dynamic viscosity
ρ	density
σ_f	Staverman filtration coefficient
υ	kinematic viscosity

Subscripts

e	effective property
L	left common iliac artery
R	right common iliac artery
a	aorta

Symbols

$\langle\rangle$	"local volume average" of a quantity

some information on the hemodynamics and its localized effects, these studies fail to provide detailed distribution of LDL concentration within the arterial wall. Some other research works utilized a more developed arterial transport model, the homogeneous porous wall model, which accounts for the wall of the artery as a homogenous porous wall [8]. This model provides a rather rough approximation of LDL concentration distribution within the wall. Nonetheless, it does not offer any information on the accurate distribution of LDL concentration within the inherently heterogeneous arterial wall.

Far more complete computational modeling [6,7] and analytical solutions [9,10] of arterial transport phenomena have been performed using the multi-layer porous wall model [8]. Analytical solutions encompassing various physical and phenomenological attributes of the macromolecular arterial transport are given in Khakpour and Vafai [9] and Yang and Vafai [10]. This model represents the arterial wall to be composed of several heterogeneous porous layers, i.e. endothelium, intima, IEL, and media. The multi-layer model is advantageous over the homogeneous-wall model in that it accounts for the particular characteristics and properties of each porous layer. As mentioned earlier, atherosclerosis is characterized as an abnormal thickening of the intima. Therefore, it is essential to investigate the interaction between arterial layers and the role of each layer in the uptake of the macromolecules and development of atherosclerosis. Use of a multi-layer model and solution of a proper set of governing equations and boundary conditions can result in an accurate description of dynamics and distribution of macromolecules across the arterial wall.

The arterial tree is a complex system. It starts off with a single artery called aorta. This main artery branches in several locations until it reaches the lower abdomen, where it bifurcates into right and left common iliac arteries. The site of the bifurcation is usually referred to as aorta–iliac bifurcation. This bifurcation has particular characteristics which are usually neglected. For instance, anatomical distinctions between the iliac arteries at the bifurcation have not received proper attention. A critical examination of this region [11] shows that the aorta at its bifurcation lies to the left of the sagittal plane midline, with the result that the right iliac artery makes a wider take-off angle, and consequently must be longer, in order to reach the right side [11]. Differences in the angle of bifurcation may directly affect the radius of curvature which in turn affects the hemodynamics and hence the predilection of atherogenesis to certain sites. Shah et. al. [11] performed quantitative anatomical measurements of aorta–iliac bifurcation and showed differences of angle at the bifurcation and radii of curvature. An important characteristic of the aorta–iliac bifurcation is the geometrical differences observed between men and women. As observed in the measurements of Shah et al. [11], the geometric differences between the two common iliac arteries at the aortic bifurcation are especially severe in males owing to the greater differences in male pelvic geometry as compared to females.

In men, due to their narrower pelvic geometry as compared to women, the left iliac artery requires a significantly smaller take-off angle. However, the bifurcation angle of the right common iliac artery is similar to that of women. This makes the asymmetry of the bifurcation even more pronounced for men, as compared to women. As such, we expect to observe considerable differences in the hemodynamical factors as well as the arterial wall uptake of macromolecules between men and women. Due to significance of the blood volumetric flow rate, a number of physiological flow rates are used. This is done to elucidate the displacement of hemodynamically critical regions and their subsequent effect on the macromolecule concentration distribution within the arterial wall.

In the present work, computational simulations of hemodynamics and macromolecule transport at an aorta–iliac bifurcation are performed. Two main distinctive characteristics of this bifurcation are investigated: asymmetry and gender-dependence of geometry. The transport phenomena within the lumen and the arterial wall are coupled. The arterial wall is modeled as a four-layer porous wall. The layers are all treated as macroscopically homogeneous porous media with uniform morphological properties. Staverman filtration coefficient is incorporated to account for selective permeability of each porous layer to macromolecules. Profiles of LDL concentration distribution are obtained for different cases. The results are discussed with regard to the shear stress distribution, which is believed to be one of the key factors in atherogenesis.

2. Formulation

The configuration under consideration is shown in Fig. 1. The luminal blood flow is assumed to be Newtonian, isothermal and incompressible. Blood properties (i.e. viscosity and diffusivity) are assumed to be constant. Navier–Stokes equations coupled with mass transport equations (advection–diffusion) are employed to solve for the luminal blood flow and solute transport. These governing equations are given by

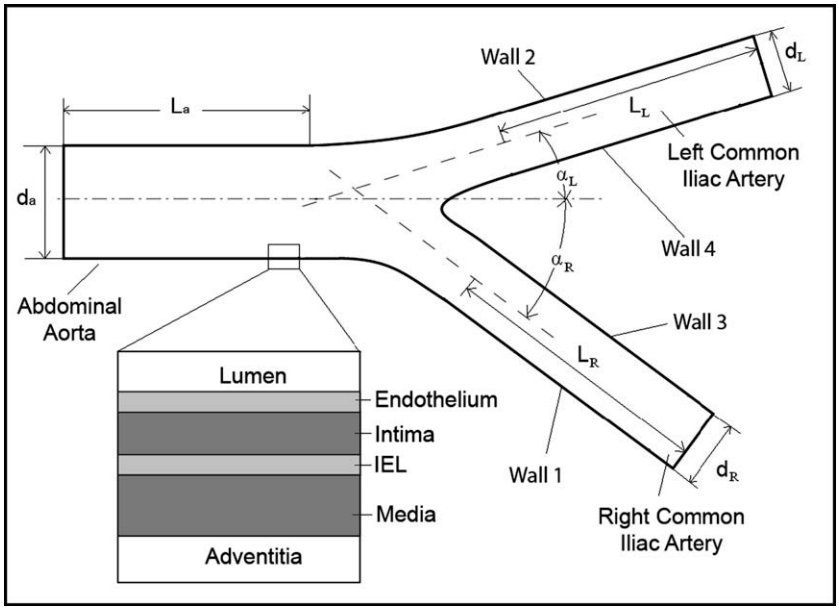

Fig. 1. Schematic illustration of the aorta–iliac bifurcation.

$$\nabla \cdot \vec{V} = 0 \tag{1}$$

$$\rho \vec{V} \cdot \nabla \vec{V} = -\nabla p + \mu \nabla^2 \vec{V} \tag{2}$$

$$\vec{V} \cdot \nabla C = D \nabla^2 C \tag{3}$$

where $\vec{V}$ is the velocity vector, p the pressure, ρ the density, μ dynamic viscosity of blood, C the solute concentration, and D is the solute diffusivity within the blood.

The Staverman filtration coefficient is incorporated to account for selective permeation of species by the membranes [6–10]. The governing equations for conservation of mass, momentum, and species concentration in the porous layers are given by

$$\nabla \cdot \langle \vec{V} \rangle = 0 \tag{4}$$

$$\nabla \langle P \rangle^{\mathrm{f}} = \frac{\mu}{\delta} \nabla^2 \langle \vec{V} \rangle - \frac{\mu}{K} \langle \vec{V} \rangle \tag{5}$$

$$(1 - \sigma_{\mathrm{f}}) \langle \vec{V} \rangle \cdot \nabla \langle C \rangle = D_{\mathrm{e}} \nabla \langle C \rangle^2 + k \langle C \rangle \tag{6}$$

where K is the permeability of the porous medium. The parameters σ_{f} and D_{e} represent the Stavernan filtration coefficient and the effective solute diffusivity in the porous medium, respectively. The effective volumetric first-order reaction rate, k, takes a value of zero for endothelium, intima, and IEL. The symbol $\langle\ \rangle$, represents the local volume average of a quantity associated with the fluid [12] and the parameter $\langle P \rangle^{\mathrm{f}}$ is the average local pressure inside the fluid. The effects of osmotic pressure on the filtration velocity are neglected based on the detailed results presented by Ai and Vafai [6] and Yang and Vafai [7].

The lumen velocity field at the aorta inlet is assumed to be laminar and fully developed. Comparisons of time-averaged flow and concentration fields with steady state results reveal that the effects of pulsation on the arterial transport phenomena is not substantial [6]. Thus, a parabolic profile is prescribed

$$u = u_{\max}[1 - (r/R)^2] \tag{7}$$

where $u_{\max}$ is the centerline (maximum) velocity, R the inner radius of the artery, u the streamwise component of the velocity vector, and r is the radial location. A continuity boundary condition is employed at the interface between the layers. This boundary condition requires the value of velocity and its derivative (equivalent to wall shear stress) to remain constant across the interface.

$$(\vec{n} \cdot \vec{V})|_{+} = (\vec{n} \cdot \vec{V})|_{-} \tag{8}$$

$$\vec{t} \cdot (\nabla \vec{V})|_{+} = \vec{t} \cdot (\nabla \vec{V})|_{-} \tag{9}$$

where $\vec{n}$ and $\vec{t}$ are the unit vectors normal and tangential to the interface, respectively. A constant pressure condition is specified at the media–adventitia interface (outer boundary of the arterial wall). The value of this pressure is taken from the literature [6,7]. At the lumen outlet boundary a zero surface traction force condition is prescribed.

$$\{p\vec{I} + \mu[\nabla \vec{V} + (\nabla \vec{V})^{\mathrm{T}}]\}.\vec{n}|_{\text{lumen outlet}} = 0 \tag{10}$$

At the inlet a uniform and constant species concentration is prescribed. The value of species concentration and the total species flux are continuous at the interfaces [6–10].

$$C|_{+} = C|_{-} \tag{11}$$

$$[\vec{n} \cdot \{(1 - \sigma_{\mathrm{f}})\vec{V}C - D_{\mathrm{e}} \nabla C\}]_{+} = [\vec{n} \cdot \{(1 - \sigma_{\mathrm{f}})\vec{V}C - D_{\mathrm{e}} \nabla C\}]_{-} \tag{12}$$

At the media–adventitia interface (outer boundary of the arterial wall), the concentration gradient in the direction normal to the interface is assumed to be negligible [7].

$$\vec{n} \cdot (D_{\mathrm{e}} \nabla C)|_{\text{media-adventitia interface}} = 0 \tag{13}$$

A thorough analysis of different types of wall boundary conditions is presented in the work of Yang and Vafai [7]. Based on this work, at the outlet of the arteries, a convective flux boundary condition (zero concentration gradient) is prescribed. Although a convective boundary condition is specified at the media–adventitia interface, the convective mass flux is negligible as shown by Yang and Vafai [7].

3. Methodology

The computational model was implemented using a finite element-based commercial code, Comsol Multiphysics. The geometrical case studies were constructed based on the data provided by Shah et. al. [11]. The dimensions and transport properties associated with the arterial layers are provided in Table 1. A mapped meshing has been utilized in the numerical simulations as it performs substantially better than triangular mesh in capturing boundary layer characteristics. The computational domain was di-

Table 1
Physiological properties of the arterial layers used in this study

	Endothelium	Intima	IEL	Media
Thickness, l (m)	2×10^{-6}	1×10^{-5}	2×10^{-6}	2×10^{-4}
Permeability, K (m^2)	4.32×10^{-21}	2.00×10^{-16}	4.392×10^{-19}	2.00×10^{-18}
Porosity, δ	0.0005	0.983	0.02	0.258
Effective diffusivity, D_e (m^2/s)	6.00×10^{-17}	5.40×10^{-12}	3.18×10^{-15}	5.00×10^{-14}
Filtration reflection coefficient, σ_f	0.9979	0.8272	0.9827	0.8836
Reaction rate coefficient, r (1/s)	0.00	0.00	0.00	3.197×10^{-4}

Table 2
Pertinent cases representing substantial variation of geometrical attributes

Case	Description	Diameter of distal aorta	Length of common iliac arteries		Diameter of common iliac arteries		Take-off angles	
			L_R	L_L	d_R	d_L	α_R	α_L
*M*0	Mean attributes for male anatomy	2.1	6.1	5.8	1.28	1.24	29	14
*F*0	Mean attributes for female anatomy	1.83	5.63	5.4	1.13	1.11	32	26
*M*1	The most asymmetric case (male)	2.1	6.1	5.8	1.28	1.24	40	0
*M*2	The symmetric case corresponding to *M*1	2.1	6.1	5.8	1.28	1.24	40	40

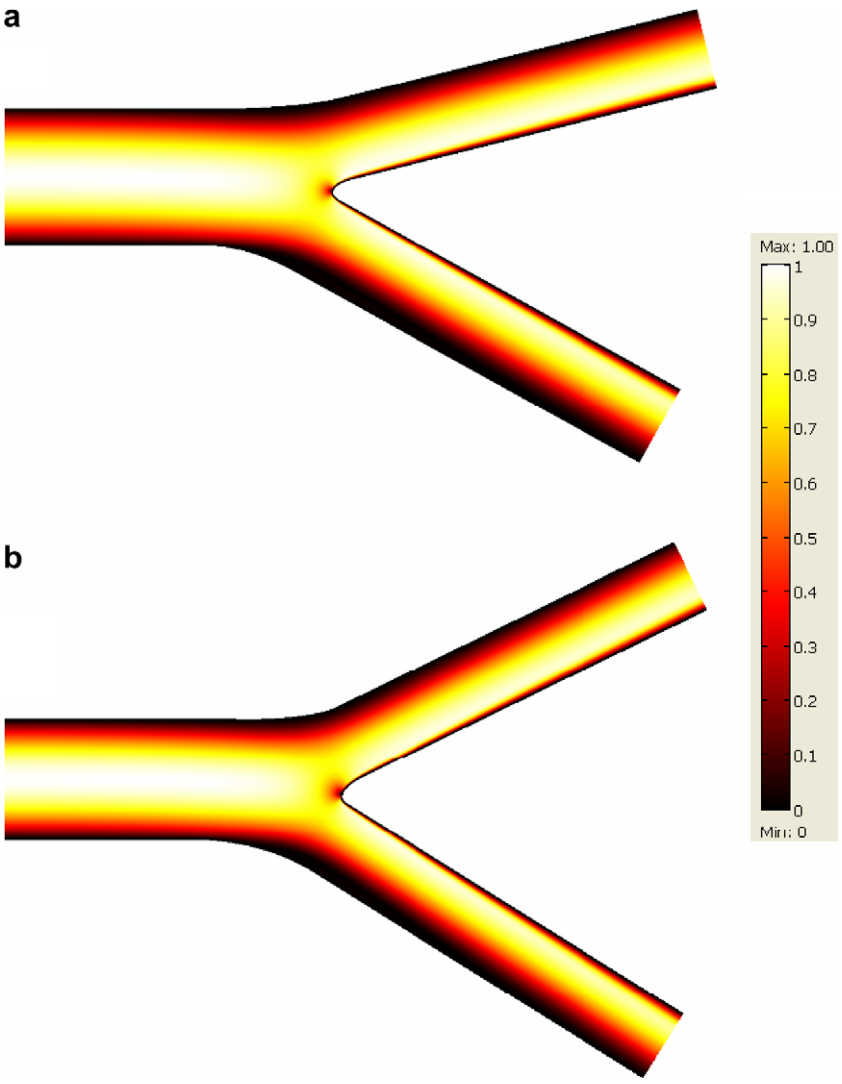

Fig. 2. Non-dimensional velocity field around the aorta–iliac bifurcation for a Reynolds number of $Re = 2000$; (a) average male geometry, (b) average female geometry.

vided into 10,640 quadrilateral elements. This resolution was arrived at by performing a grid-refinement study. The resolution was continually increased until (a) there were no changes in the velocity field and the species concentrations and (b) the species concentration profiles were oscillation-free. The mesh quality (aspect ratio) has also been monitored to facilitate the convergence and to ensure the accuracy of the results. Due to high Peclet number (convection-dominated) nature of the phenomenon, the Galerkin finite element method becomes unstable, resulting in spurious oscillations. As such, a streamline upwind Petrov–Galerkin method (SUPG) [13] is employed.

4. Results and discussion

Statistical anatomical data [11] are used to generate the bifurcation geometries. A total of four pertinent cases, representing variations of geometrical attributes, are modeled. Geometrical data used in these cases, referred to as *F*0, *M*0, *M*1, and *M*2, are provided in Table 2. Cases *F*0 and *M*0 represent the average female and male bifurcation geometries, respectively. The bifurcation angles of right and left common iliac arteries for an average male anatomy are 29° and 14°, respectively. However, the average right and left female iliac bifurcation angles are reported to be 32° and 26°, respectively.

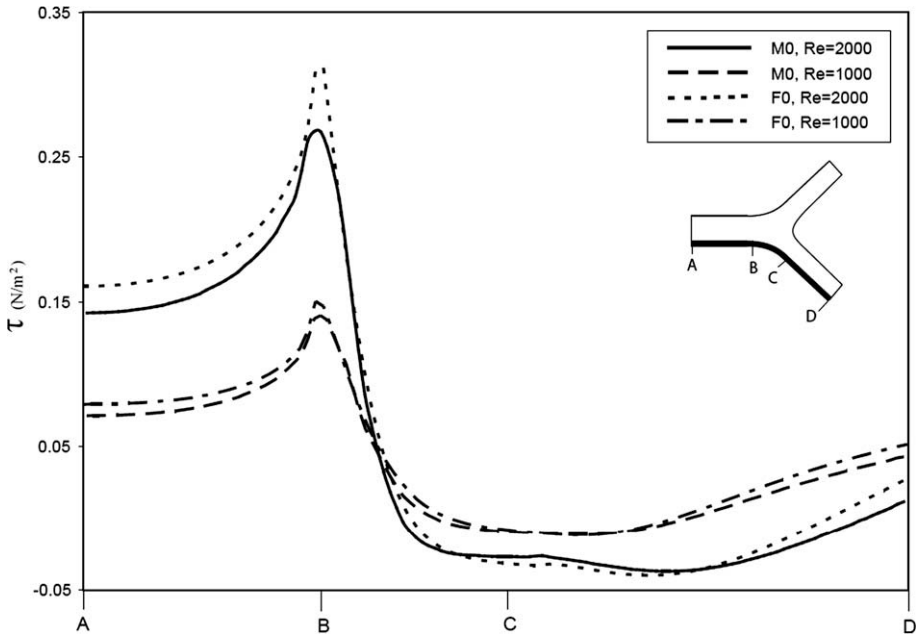

Fig. 3. Shear stress distribution along the inner lower wall of the aorta–iliac bifurcation for both men and women.

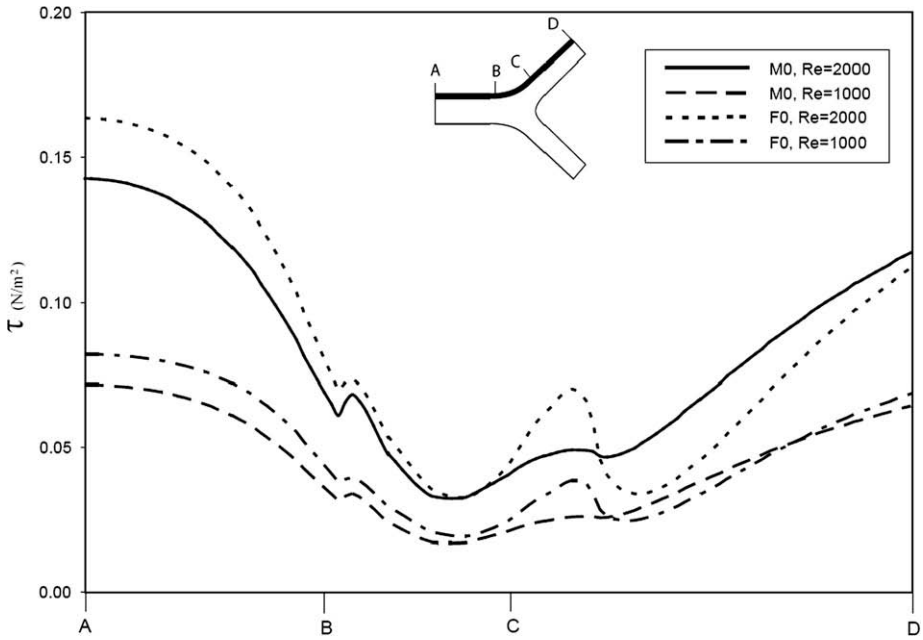

Fig. 4. Shear stress distribution along the inner upper wall of the aorta–iliac bifurcation for both men and women.

Comparing these average values, the following conclusions can be made: (1) the bifurcation angles are larger for female anatomy; (2) the difference between the right and left take-off angles is higher for men (107%) than for women (23%). The latter indicates more symmetry for the female bifurcation structure as compared to that of male. It should be noted that the above arguments are based solely on average geometrical data. The asymmetry of the bifurcation arises not only because of differences in iliac arteries' take-off angles but also due to the difference in the radius of curvature for each iliac artery [11]. Based on the geometrical data, the left common iliac artery takes off with a larger radius of curvature as compared with right common iliac artery.

To further investigate the effects of asymmetry on the hemodynamics and eventually macromolecule transport, the most asymmetric case reported by Shah et al. is chosen. Note that this case, *M*1, refers to the most asymmetric case, not the average data. In this case the bifurcation angles of right and left common iliac arteries for average male anatomy are 40° and 0°, respectively. For the sake of comparison, a perfectly symmetric case has also been modeled. This case, *M*2, is symmetric with respect to aorta's center line. As such, the left common iliac artery has the same radius of curvature, axial location and angle of bifurcation as the right common iliac artery. It bears mentioning that this case does not correspond to real data and is made for comparison purposes only.

The lumen velocity and the diameter of aorta are different between men and women. As such, to obtain a fair comparison, cases are run for the same Reynolds number. Each case is run for two different values of Reynolds number, *Re*, which is defined as

$$Re = \frac{u_m d_a}{\upsilon} \tag{14}$$

where u_m and d_a are the mean velocity and diameter of aorta before bifurcation and υ is the kinematic viscosity of blood. The values of Reynolds number are chosen to represent the blood flow both at rest and exercise. In what follows, the two main features of the aorta–iliac bifurcation are analyzed: gender-related geometrical differences and asymmetry.

Fig. 2 shows the steady state contours of the velocity field for an average male and average female aorta–iliac bifurcation. The corresponding Reynolds number is *Re* = 2000 and the velocity is nondimensionalized based on its centerline value at the inlet. The darkest and lightest shades represent the minimum (zero) and maximum (unity) values, respectively. Within the aorta, where the velocity profile is parabolic, the maximum velocity is observed

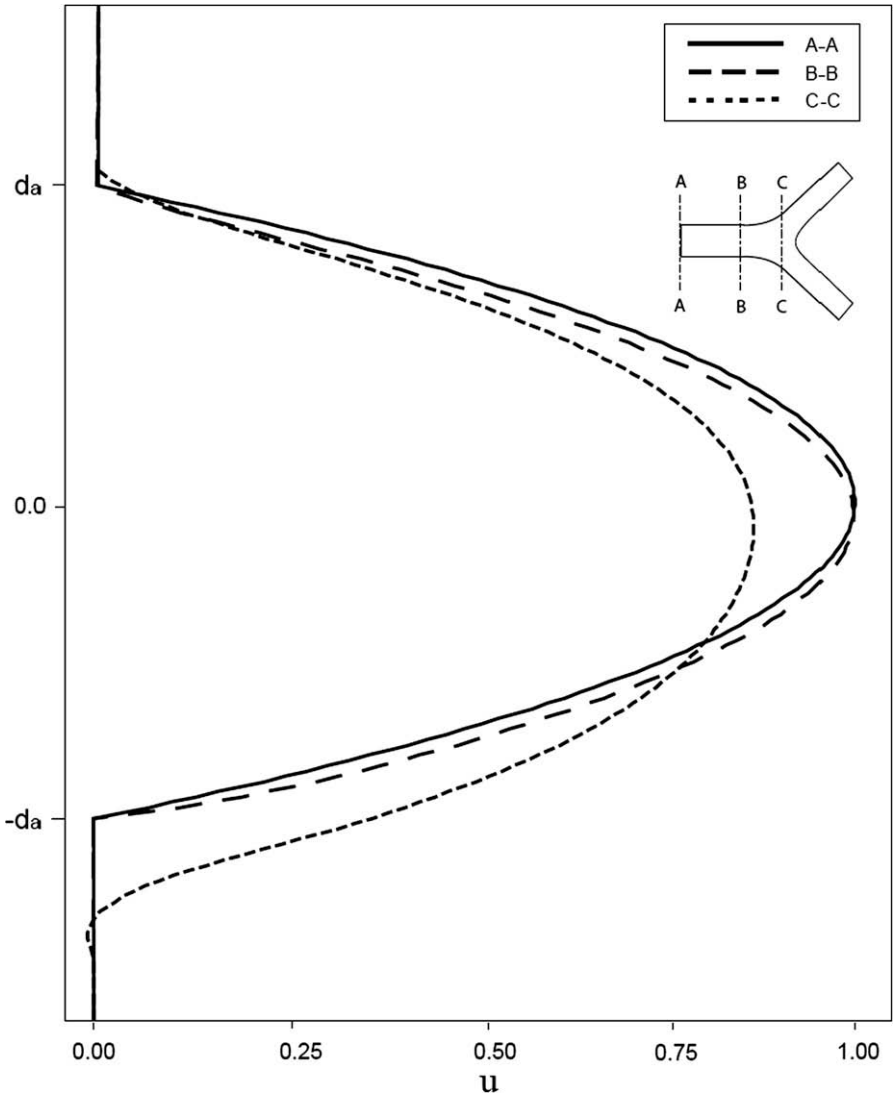

Fig. 5. Axial variations of the *x* component of the velocity field along the aorta.

in the middle. Within the common iliac arteries, the maximum value of velocity profile is observed close to walls 3 and 4 (Fig. 1). This exerts a significantly higher shear stress on walls 3 and 4 as compared to walls 1 and 2.

4.1. Gender

Fig. 3 shows the wall shear stress distribution along the endothelial surface of the wall midsection of the right common iliac artery (wall 1) for men and women at two different Reynolds numbers. The magnitude of the wall shear stress increases in the vicinity of the bifurcation with a peak roughly at the location where the curvature starts. It then drops drastically resulting in a change in the direction of the wall shear stress. This is an indication of flow separation along the curvature. The Reynolds number is seen to have a significant effect on the magnitude of wall shear stress. Higher Reynolds numbers cause an increase in the length of the recirculation region where the minimum value of wall shear stress occurs. Fig. 3 shows that the wall shear stress on wall 1 is slightly (maximum of 7% and 17% for $Re = 1000$ and $Re = 2000$, respectively) higher for average female bifurcation as compared to that of an average male. Also, the length of the recirculation region on wall 1 is slightly shorter for an average female bifurcation compared to that of a male.

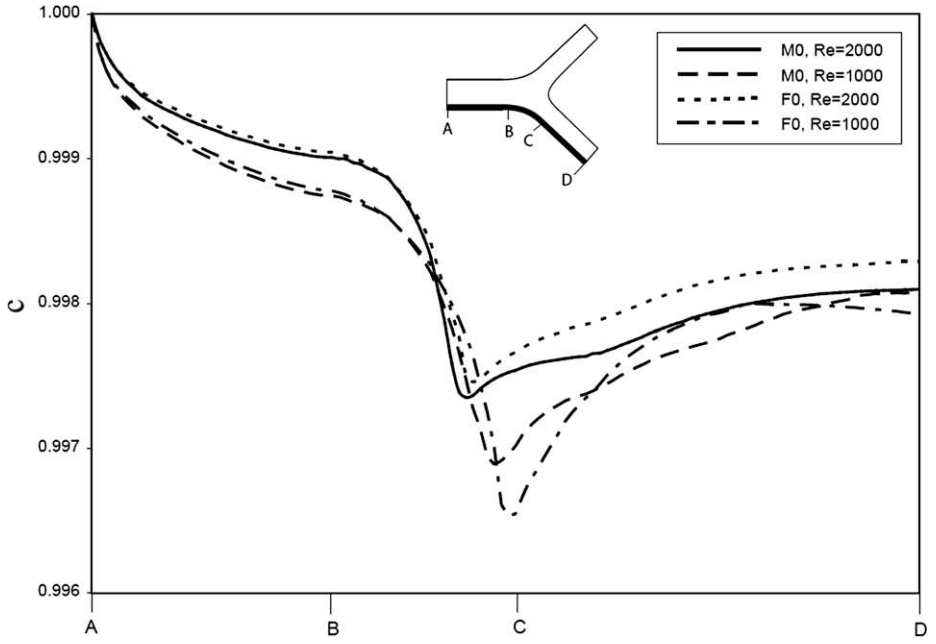

Fig. 6. Macromolecule concentration distribution along the inner lower wall of the aorta–iliac bifurcation for both men and women.

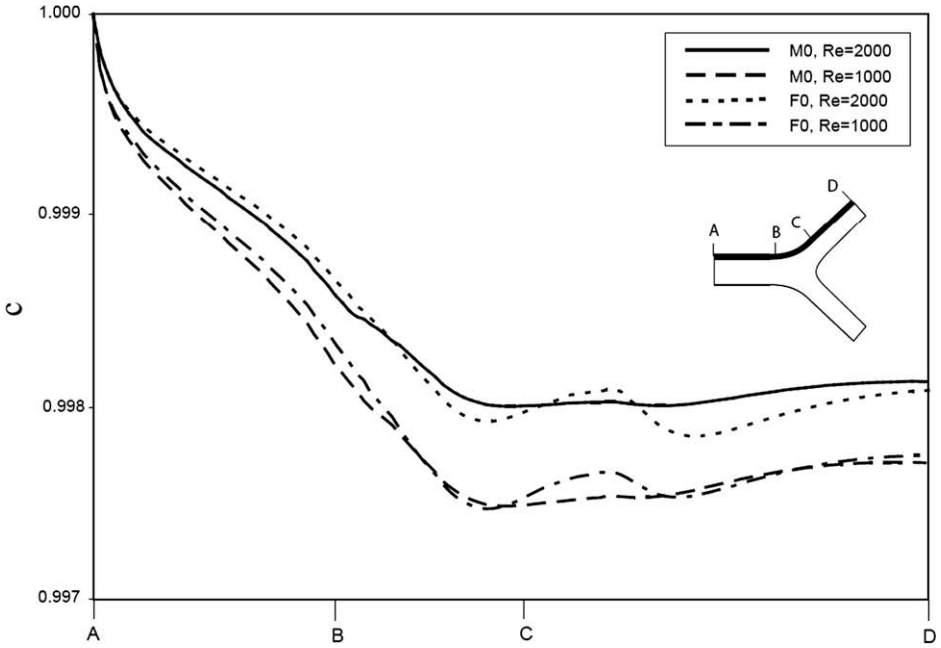

Fig. 7. Macromolecule concentration distribution along the inner upper wall of the aorta–iliac bifurcation for both men and women.

Fig. 4 presents the wall shear stress distribution along the endothelial surface of the midsection of the left common iliac artery (wall 2) for men and women at two different Reynolds numbers. Moving from the inlet towards the bifurcation, the wall shear stress decreases with its minimum value occurring around the mid-point of the curvature. It then increases as it moves along the left common iliac artery. The decrease along the aorta is believed to be due to a change in the velocity profile. As shown in Fig. 5, the streamwise component of the velocity field starts as a symmetric parabolic profile. However, due to asymmetric structure of the bifurcation, the profile looses its symmetry and inclines towards the right. This results in an increase in the wall shear stress on aortic part of wall 1, while reducing it on aortic part of wall 2, as shown in Figs. 3 and 4. Two local maxima are observed in wall shear stress profile of wall 2. These are caused by abrupt changes in velocity profile due to bifurcation. It is observed that for the same Reynolds number, the magnitude of wall shear stress is higher for women. Also, the local maxima are more pronounced for women as the bifurcation is wider and the velocity field undergoes a more substantial change.

Fig. 6 presents the macromolecule concentration distribution along the endothelial surface of wall 1 for men and women at two different Reynolds numbers. Due to chemical reaction within the media layer, the concentration decreases from its initial value. Along the curvature, between points B and C, the concentration profile experiences a relatively sharp decrease. This is due to existence of the low velocity recirculation region which acts in maintaining and recirculating the same fluid in that region, cutting off

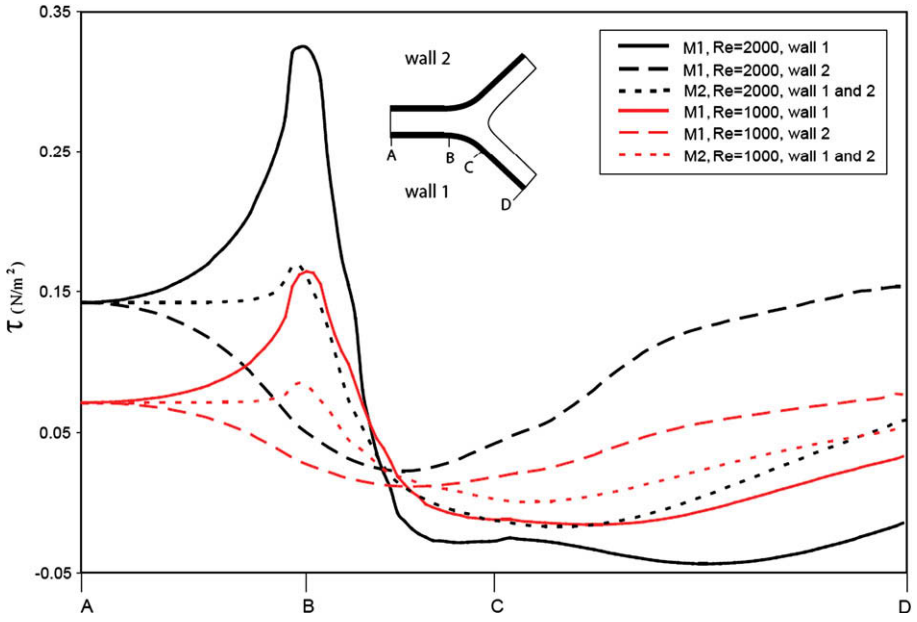

Fig. 8. Shear stress distribution along the inner wall of the aorta–iliac bifurcation. A comparison between a highly asymmetric case and a perfectly symmetric case.

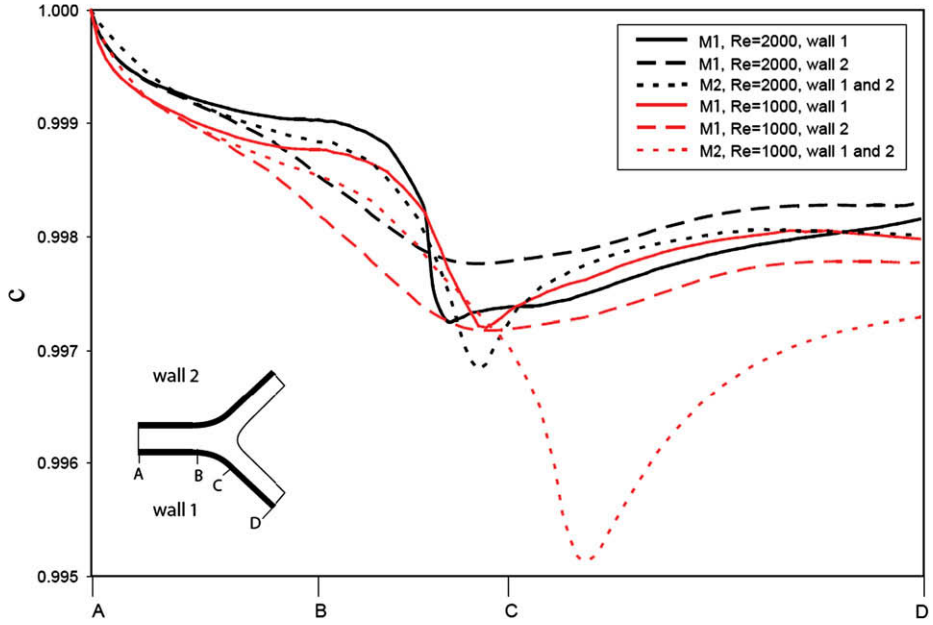

Fig. 9. Macromolecule concentration along the inner wall of the aorta–iliac bifurcation. A comparison between a highly asymmetric case and a perfectly symmetric case.

Table 3
Summary of some key observations

	Wall shear stress	Macromolecule concentration
Lumen flow rate	(1) Increase in lumen flow rate results in an increase in the magnitude of wall shear stress (2) Increase in Reynolds number increases the length of the recirculation region along the right common iliac artery	Increase in lumen flow rate results in an increase in the wall macromolecule concentration
Gender	For the same lumen flow rate, an average female geometry has: (1) A slightly higher wall shear stress (2) A slightly shorter recirculation region	No significant effect was observed
Asymmetry	For the same lumen flow rate, asymmetry results in: (1) Higher magnitude of shear stress along the right common iliac artery (2) Smoother shear stress profile along the left common iliac artery	For the same lumen flow rate, asymmetry results in: (1) Higher magnitude of shear stress along the right common iliac artery (2) Smoother and slightly higher concentration along the left common iliac artery

the macromolecule supply from the free stream towards to endothelial surface. As such, macromolecules contained in the recirculating fluid are consumed, and with a much lower supply from the free stream, a relatively sharp decrease in concentration on the endothelial surface results. Moving down the right common iliac artery, as the recirculation region gets smaller and weaker, the wall macromolecule concentration increases. Fig. 7 represents the macromolecule concentration distribution along the endothelial surface of wall 2 for men and women at two different Reynolds numbers. Similar to Fig. 6, macromolecule concentration decreases on the aortic wall. However, it remains relatively constant as this wall does not experience a major flow separation and recirculation region. In both figures, it is observed that higher Reynolds numbers result in higher wall concentrations. Also, macromolecule concentration profile for a female bifurcation on wall 2 experiences a local maximum around the same location where the major local maximum of wall shear stress occurs (Fig. 4). No other significant difference is observed between the wall macromolecule concentration of male and female anatomy.

4.2. Asymmetry

Fig. 8 shows the distribution of shear stress along the inner walls of the aorta–iliac bifurcation. For case *M*1, the shear stress remains somewhat constant along the aorta, but along the right common iliac artery, it increases significantly as it approaches the bifurcation point and drops suddenly afterwards. This sudden drop was previously shown to be the result of flow separation and creation of a recirculation region. The separation also changes the direction of wall shear stress, but the sign (direction) changes again as the recirculation region ends. Wall 2, exhibits a somewhat different variation of wall shear stress as it bifurcates. As shown in Fig. 8, the wall shear stress drops smoothly along the curvature and then increases as the curvature ends. For the symmetric case, *M*2, the profiles of wall shear stress become identical along the two walls. For a given Reynolds number, the variation of shear stress profile for the *M*2 case is similar to that of wall 1 for the *M*1 case, but with smaller magnitudes. It should also be noted that symmetry results in a decrease in the length of the recirculation region. Fig. 9 shows the macromolecule concentration distribution along the endothelium surface for both the right and left common iliac arteries for the asymmetric, *M*1, and its corresponding symmetric case, *M*2. For the *M*1 case, the concentration profiles follow similar trends as the ones observed in Figs. 6 and 7. For the case *M*2 however, a significant drop in concentration is observed after the curvature for the lower Reynolds number.

Although vascular behavior is dependent on both genetic and systemic factors, the majority of pathobiologic manifestations of

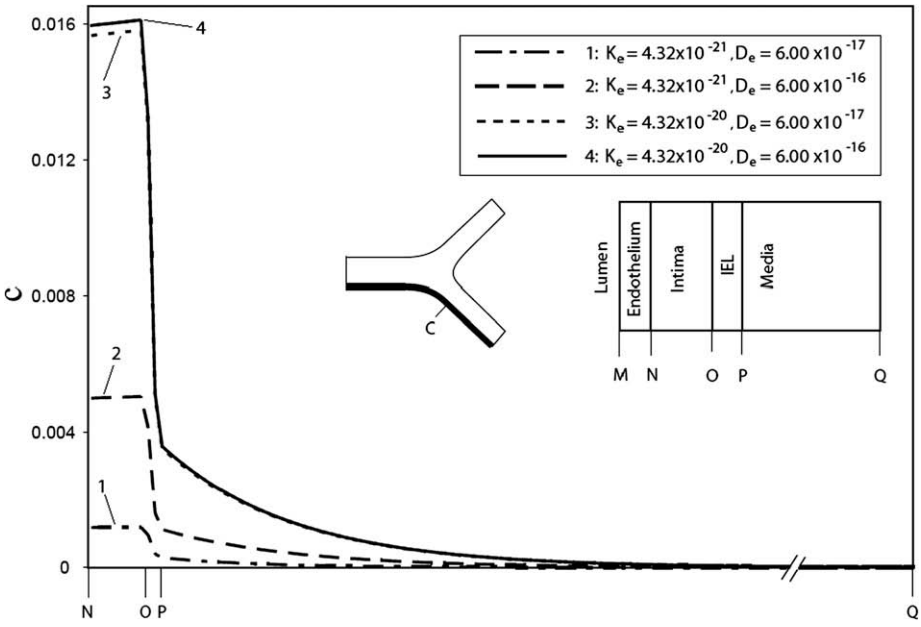

Fig. 10. Macromolecule concentration across the arterial wall after the bifurcation curvature (point C) for the case *F*0, accounting for the changes in permeability and diffusivity of endothelium. Note: Line 1 represents the normal endothelial properties.

atherosclerosis are highly focal, reflecting the critical role of local endothelial behavior [5]. It is generally accepted that regions with low and oscillating shear stress are most susceptible to atherogenesis [14–18]. A clear understanding of the effects of shear stress on the behavior and functionality of endothelial cells is still missing. This is of great importance specifically in the evaluation of transport properties for the endothelial layer. For instance, there are no well established relationships describing the changes in endothelial permeability to macromolecules when shear stress varies significantly. Such relationships are important in obtaining a more accurate concentration distribution of macromolecules within the arterial layers. Findings suggest that low wall shear stress is one of the key causes of endothelial dysfunction [19–22], which in turn results in a significantly increased endothelial permeability and diffusivity to macromolecules. A summary of these observations is provided in Table 3.

Fig. 10 shows the macromolecule concentration distribution across the arterial wall after the bifurcation curvature ends (point C) for an average female bifurcation (*F*0). Using the available data in the literature [5,14–24], increased values of endothelial permeability and diffusivity are employed for the low shear stress region. It is observed that an order of magnitude increase in endothelial diffusivity results in roughly 230% increase in intimal macromolecule concentration. On the other hand, an order of magnitude increase in endothelial permeability results in 810% increase in intimal macromolecule concentration. Combined increases in both permeability and diffusivity however, increase the intimal macromolecule concentration by 830%. This clearly shows the importance of endothelial properties in controlling the macromolecule concentration within intima, which is the site of lipid accumulation.

5. Conclusions

An investigation of blood flow and macromolecule transport at the aorta–iliac bifurcation is presented in this work. The transport phenomena within the lumen and the arterial wall are coupled. The arterial wall is modeled as a four-layer porous wall, representing endothelium, intima, IEL, and media layers. The layers are all treated as macroscopically homogeneous porous media with uniform morphological properties. The Staverman filtration coefficient is incorporated to account for selective permeability of each porous layer to macromolecules. High concentration of macromolecules such as low-density lipoprotein at the lumen–endothelium interface has been shown to play a key role in the development of atherosclerosis. Assuming constant endothelial properties, we have demonstrated that within regions of low shear stress (recirculation), the concentration decreases. However, only a maximum of 0.5% decrease was observed. As the endothelial dysfunction develops in the regions of low wall shear stress, the leaky junctions expand and the endothelial permeability and diffusivity increase. As shown in Fig. 10, this change in endothelial property may result in a substantially higher macromolecule concentration within intima, which is the site of formation of atheroma. Different geometrical attributes of the aorta–iliac bifurcation are studied, such as asymmetry and gender-dependence. Profiles of wall shear stress and macromolecule concentration distribution are analyzed for different cases. Comparisons between hemodynamics of an average male and female aorta–iliac bifurcation reveal higher magnitude of wall shear stress in females. Also, both wall shear stress and wall macromolecule concentration profiles seem to be more uniform in an average male geometry. Asymmetry is shown to have a significant effect on both wall shear stress and macromolecule concentration distributions. The differences in radius of curvature, takeoff angle, and specifically the bifurcation point makes the right common iliac artery hemodynamically more susceptible to development of atherosclerosis. It should be noted that the results are based on average geometries and gender differences thus providing a statistical basis for analyzing some of the important attributes. Finally, changes in endothelial permeability and macromolecule diffusivity, caused by endothelial dysfunction, are shown to have a substantial influence on macromolecule concentration within intima, which is the site of lipid accumulation. The results emphasize the importance of accurate evaluation of endothelial properties as a function of shear stress.

References

[1] American Heart Association Heart Disease and Stroke Statistics-2007 Update, American Heart Association, Dallas, TX, 2007.
[2] H. Stary, A. Chandler, R. Dinsmore, V. Fuster, S. Glagov, W. Insull Jr., M. Rosenfeld, C. Schwartz, W. Wagner, R. Wissler, A definition of advanced types of atherosclerotic lesions and a histological classification of atherosclerosis: a report from the committee on vascular lesions of the council on arteriosclerosis, Am. Heart Assoc. Circul. 92 (1995) 1355–1374.
[3] C. Glass, J. Witztum, Atherosclerosis: the road ahead, Cell 104 (2001) 503–516.
[4] S. Frangos, V. Gahtan, B. Sumpio, Localization of atherosclerosis role of hemodynamics, Arch. Surg. 134 (1999) 1142–1149.
[5] P. Stone, A. Coskun, S. Kinlay, J. Popma, M. Sonka, A. Wahle, Y. Yeghiazarians, C. Maynard, R. Kuntz, C. Feldman, Regions of low endothelial shear stress are the sites where coronary plaque progresses and vascular remodelling occurs in humans: an in vivo serial study, Eur. Heart J. 28 (2007) 705–710.
[6] L. Ai, K. Vafai, A coupling model for macromolecule transport in a stenosed arterial wall, Int. J. Heat Mass Transfer 49 (2006) 1568–1591.
[7] N. Yang, K. Vafai, Modeling of low density lipoprotein (ldl) transport in the artery – effects of hypertension, Int. J. Heat Mass Transfer 49 (2006) 850–867.
[8] M. Khakpour, K. Vafai, Critical assessment of arterial transport models, Int. J. Heat Mass Transfer 51 (2008) 807–822.
[9] M. Khakpour, K. Vafai, A comprehensive analytical solution of macromolecule transport within an artery, Int. J. Heat Mass Transfer 51 (2008) 2905–2913.
[10] N. Yang, K. Vafai, Low-density lipoprotein (ldl) transport in an artery – a simplified analytical solution, Int. J. Heat Mass Transfer 51 (2008) 497–505.
[11] P. Shah, H. Scarton, M. Tsapogas, Geometric anatomy of the aortic-common iliac bifurcation, J. Anat. 126 (1978) 451–458.
[12] B. Alazmi, K. Vafai, Analysis of variants within the porous media transport models, ASME J. Heat Transfer 122 (2000) 303–326.
[13] A. Brooks, T. Hughes, Streamline upwind/Petrov–Galerkin formulations for convection dominated flows with particular emphasis on the incompressible Navier–Stokes equations, Comput. Methods Appl. Mech. Eng. (1999) 199–259.
[14] W. Stehbens, The role of hemodynamics in the pathogenesis of atherosclerosis, Prog. Cardiovasc. Dis. 18 (1975) 89–103.
[15] A. Malek, S. Alper, S. Izumo, Hemodynamic shear stress and its role in atherosclerosis, JAMA 282 (1999) 2035–2042.
[16] A. Shaaban, A. Duerinckx, Wall shear stress and early atherosclerosis: a review, Am. J. Roentgenol. 174 (2000) 1657–1665.
[17] S. Glagov, C. Zarins, D. Giddens, D. Ku, Hemodynamics and atherosclerosis. Insights and perspectives gained from studies of human arteries, Arch. Pathol. Lab. Med. 112 (1988) 1018–1031.
[18] J. Suo, D. Ferrara, D. Sorescu, R. Guldberg, W. Taylor, D. Giddens, Hemodynamic shear stresses in mouse aortas: implications for atherogenesis, Arterioscle. Thromb. Vasc. Biol. 27 (2007) 346–351.
[19] J. Davignon, P. Ganz, Role of endothelial dysfunction in atherosclerosis, Circulation 109 (2004) III-27–III-32.
[20] P. Bonetti, L. Lerman, A. Lerman, Endothelial dysfunction – a marker of atherosclerotic risk, Arterioscle. Thromb. Vasc. Biol. 23 (2003) 168–175.
[21] D. Endemann, E. Schiffrin, Endothelial dysfunction, J. Am. Soc. Nephrol. 15 (2004) 1983–1992.
[22] R. Esper, A. Nordaby, J. Vilariño, A. Paragano, J. Cacharrón, R. Machado, Endothelial dysfunction: a comprehensive appraisal, Cardiovasc. Diabetol. 5 (2006).
[23] E. Renkin, F. Curry, Endothelial permeability: pathways and modulations, Ann. NY Acad. Sci. (1982) 248–258.
[24] N. Resnick, H. Yahav, A. Shay-Salit, M. Shushy, S. Schubert, L. Chen, M. Zilberman, E. Wofovitz, Fluid shear stress and the vascular endothelium: for better and for worse, Progr. Biophys. Mol. Biol. 81 (2003) 177–199.